HEDL-SA-1521

CONF-780829--1

MASTER

RECENT ADVANCES IN FEATURE EXTRACTION TECHNIQUES BEING DEVELOPED FOR ULTRASONIC EXAMINATION OF AUSTENITIC STAINLESS STEEL WELDS

S.J. Mech, J.S. Emmons
and T.E. Michaels

August 1978

Society of Photo-Optical
Instrumentation Engineers

San Diego, California
August 28-31, 1978

HANFORD ENGINEERING DEVELOPMENT LABORATORY
Operated by Westinghouse Hanford Company, a subsidiary of
Westinghouse Electric Corporation, under the Department of
Energy Contract No. EY-76-C-14-2170

RECENT ADVANCES IN FEATURE EXTRACTION TECHNIQUES BEING DEVELOPED FOR ULTRASONIC EXAMINATION OF AUSTENITIC STAINLESS STEEL WELDS

S. J. Mech, J. S. Emmons, and T. E. Michaels
Hanford Engineering Development Laboratory
Richland, Washington 99352

Abstract

This paper describes techniques being developed to characterize the features found during ultrasonic examination of stainless steel welds which are indicative of defects. Ultrasonic waveforms obtained from both defects and grain boundaries have similar time-domain characteristics. This phenomenon, together with variable signal attenuation and dispersion, is commonly encountered. The problem is to develop feature extraction techniques which will enable the examiner to discriminate reliably between weld defect signals and the other noise. Techniques presented use both time and frequency domain algorithms. The use of these techniques has demonstrated significantly better discrimination than conventional ultrasonic methods.

Introduction

Development of more effective methods for ultrasonic examination of welds in austenitic stainless steel components is an important objective in the nuclear industry. The specific objective of this program is to develop ultrasonic methods for pre-service and in-service inspection of austenitic stainless steel welds in certain Fast Flux Test Facility (FFTF) pipes.

The challenge is to develop techniques which find defects but ignore variations associated with the normal cast type microstructure of the weld zone. This study was directed at gathering data on a welded pipe section with notches used to simulate defects, and is another example of computer acquisition and analysis techniques of ultrasonic data[1]. Various analysis methods were compared to find signal analysis algorithms sensitive to these simulated defects. For the overall problem, we classify algorithms in two broad categories. First, we need an inspection scheme to quickly scan a section to find all potential defect locations. In the second category, we need techniques to classify signals in order to size defects identified by the first method. This report discusses results for the first category.

Austenitic Stainless Steel Microstructure

For austenitic stainless steel welds, the microstructure dominates the wave propagation response[2]. The weld zone is characterized by large columnar grains (dendrites) which result from the slow cooling and directional solidification during welding. Wave velocities and propagation modes within these dendrites exhibit anisotropy which is describable by well known relations derived for face-centered-cubic crystal structure, i.e., austenite phase. These variations in wave velocity with crystallographic direction produce large acoustic impedance differences at grain boundaries.

A substantial portion of the ultrasonic beam is reflected by the local impedance changes at grain boundaries. These reflections develop signal responses often described as "grain noise," and this "grain noise" is frequently as pronounced as echoes from large cross sectional flaws within the weld zone for austenitic stainless steel[3]. Correspondingly, grain noise may be reported as defects, while actual defects may be difficult to locate during inspection. This is because energy reflected from defects is often not directed towards the discrete location of transducers.

Figure 1 illustrates these effects. Relative to the signal obtained from the reference defect in the parent material (a), the two signals from an identical defect (b & c) in the welded zone are of significantly lower amplitude. When the system gain is increased to 60 db, such that the observed amplitudes are comparable to the reference, (d) illustrates an ideal signal, (e) exhibits a loss of reflected energy, and (f) is "grain noise." All of these signals, except (e), are from reference defect. Signal (e) was obtained from a volume with no defects.

Many methods can be used to enhance defect signals and suppress grain noise for austenitic stainless steel weld inspection. Inspecting at lower frequencies reduces grain noise[4]. Grain scatter is less pronounced at lower frequencies where wavelength is much greater than grain size; however, sensitivity to small defects is also reduced. It is often a necessary and laborious step to select a frequency range high enough to see small defects yet low

enough to minimize grain noise. Also, the orientation of dendrites is known to have the principal axis pointing towards the center of the weld zone. Thus, there may be propagation directions along which grain scatter is minimal[5,6,7]. All these approaches are useful, but all grains are not found to be the same size nor are they aligned in the same direction. Instead, the weld zone is a mixture of size, shapes, and preferred orientations of many microconstituents.

If the test is tailored to the nominal microstructure, then critical flaws may be missed where microstructure variations are severe. If broad weld inspection standards are to be set and met in practice, the evaluation method should be as microstructurally insensitive as practical. A significant improvement in this area has been made, and is the subject of this paper.

Data Acquisition and Analysis System

An ultrasonic automatic data processing system (UT/ADP) was developed and used to objectively gather waveforms for analysis. The system, employing a minicomputer, was designed to permit mechanical replication of scans by accurate computer control of transducer positions. In addition, we have ability to retrieve previous scans from stored data files, thus various analysis schemes can be exercised on the same set of waveform data.

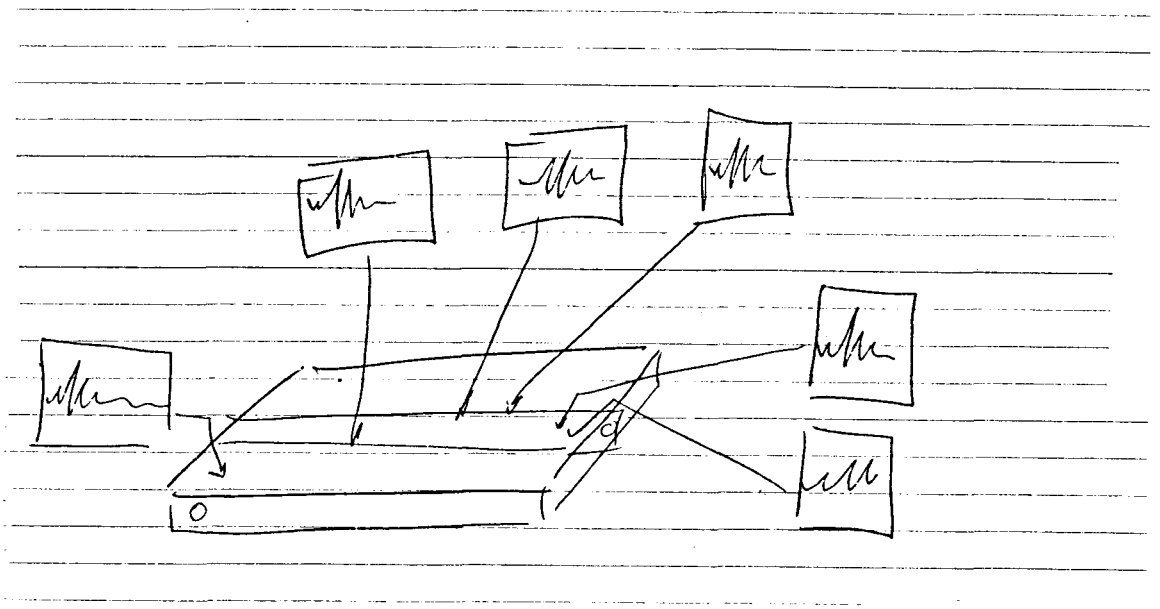

Fig. 1. Representative Ultrasonic Signals as a Function of Location.

Specimen and Data Acquisition Techniques

An austenitic stainless steel pipe section, 8-in. diameter Schedule 40, was notched at several locations to simulate defects in the weld. As illustrated in Figure 2, these notches were electro-discharge machined (EDM) 25% and 50% through the wall thickness at three orientations. The notched pipe was scanned using longitudinal and shear immersion inspection methods. The transducer was a 3 MHz, 80% bandwidth, dual-element unit (1/4-in. x 1/4-in. square) and it was designed to operate in a side-by-side pitch-catch mode. The angle between

transmit and receive beams was approximately 10° in stainless steel. This technique is similar to those used by others for austenitic stainless steel weld inspection[8,9]

The beam path illustrated in Figure 2, and was aligned to give peak return from the large center weld notch, i.e., Type C-50%. Time on the digitized records corresponded to position from the inner surface through the weld zone to the outer surface. Five-hundred waveforms were digitized and stored for one circumferential traverse around the tube. Each waveform was stored as 512 words (16 bits each), corresponding to a 20 microsecond record length.

Data Analysis Techniques

Digitized time domain waveforms were processed by three cumputational methods. These were by detecting amplitude, by cross-correlating to a waveform from a known broadband discontinuity, and by transforming to the frequency domain using a fast fourier transform (FFT) algorithm. Output of these analyses were used to train an adaptive learning network sensitive to known defect locations.

Peak Amplitude

Time domain amplitudes were computed using:

$$V_i = \max \{|v_j| : j = 4i-3, \ldots, 4i\} , \tag{1}$$

where i = 1, ..., 128, V is the amplitude waveform, and V_i replaces four data points of the RF waveform, v_j, by the peak amplitude in the internal $\{j = 4i-3, \ldots, 4i\}$. This calculation reduces the number of points per record from 512 to 128, which reduces storage requirements when only detected amplitude results are desired.

Equation (1) has the effect of full-wave rectifying and smoothing the RF waveform. This was developed to produce a result suitable for isometric plots which are presented later. It is similar to amplitude detection performed with conventional ultrasonic testing hardware.

Cross-Correlation

The cross-correlation algorithm may be used to determine where two waveforms agree or align in detail[10,11]. Specifically, it can be used to determine if, or where, a known echo pattern is contained in a noisy waveform record. Cross-correlation is useful for two reasons. First, it can be used to produce a time domain plot of echo amplitudes versus time which contains less clutter than the result of Equation (1), and this will be demonstrated in this study. Second, cross-correlation can be used to indicate where echo activity is in the time domain, which may then be used for the purpose of setting waveform gate times. This second aspect was not used in this study but is expected to be an important step in analysis in the future.

We compute cross-correlation according to:

$$W_k(A,B) = \frac{\sum_{i,j=1}^{N} A_i B_j \, \delta_{i,j+k}}{\sum_{i,j=1}^{N} \delta_{i,j+k}} . \tag{2}$$

Here δ is the Kronecker delta defined as:

$$\delta_{mn} = 1 \text{ for } m=n, \qquad \delta_{mn} = 0 \text{ for } m \neq n. \tag{3}$$

N = 512 is the number of points in the digitized waveform, W is the cross-correlation results, and k is an offset position index. This offset corresponds to sliding waveform B past waveform A, and peaks in W result for offsets where A and B align.

For analysis here, B was the echo from a back corner reflection from a calibration block, and A represents received RF waveforms. Typical results are shown in Figure 3. The position of the peak indicates where each pair aligns best. If more than one peak occurs in the cross-correlation result, these peaks indicate the probable echo locations on the original waveform.

For plotting purposes, a peak amplitude form of W is useful. This was computed using a procedure similar to that used for Equation (1):

$$\omega_{\ell}(A,B) = \max \{|W_j(A,B)| : j=4\ell-3, \ldots, 4\ell\} , \quad (4)$$

with ℓ = -64, ..., 64; and ω is peak amplitude result of the cross-correlation function. When ℓ ranges from -64 to 64, offset time ranges from -10 μsec to 10 μsec.

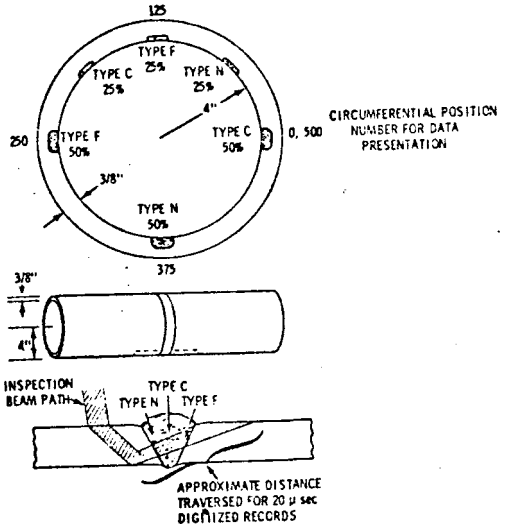

Fig. 2. Inspection Beam Path and Notch Location.

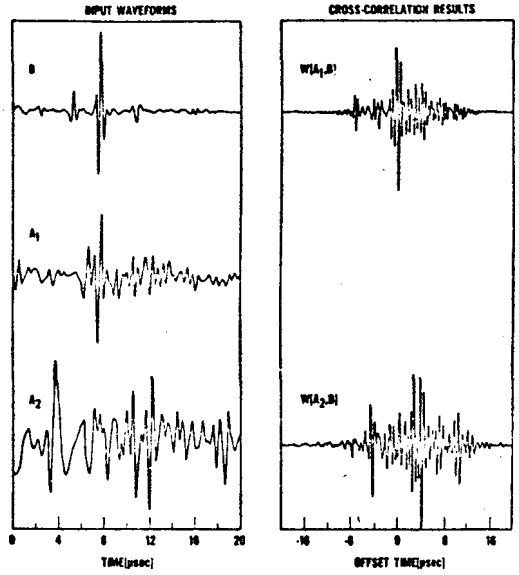

Fig. 3. Example Cross-Correlation Results.

Frequency Domain Analysis

The FFT algorithm was used to analyze the frequency content of received waveforms[12]. From this algorithm, coefficients A_ω and B_ω are related to the time domain waveform by:

$$f(t) = \int_0^\infty (A_\omega \cos \omega t + B_\omega \sin \omega t)dt, \quad (5)$$

and the power spectral density is:

$$p(\omega) = (A_\omega^2 + B_\omega^2)^{1/2} . \quad (6)$$

Simple moments are useful for comparing frequency distributions:

$$M_o = \int_0^\infty p(\omega)\ d\omega \quad (7)$$

$$M_1 = \int_0^\infty \omega p(\omega)\ d\omega \quad (8)$$

$$M_2 = \int_0^\infty \omega^2 p(\omega)\ d\omega \quad (9)$$

The zeroth moment, M_o, is equivalent to the total power. Further, by differentiating Eq. (5) with respect to time, one can show that M_1 and M_2 are related to the total power of the first and second derivative with respect to time of the original time domain waveform. This is also a standard deviation theorem for fourier transforms[13].

We found the cumulative definite integral with variable upper limit, ω, useful for detailed study of the frequency patterns from defects. This may be expressed as:

$$M_k(\omega) = \int_0^\infty \xi^k \, p(\xi) \, d\xi \ . \tag{10}$$

In discrete form this becomes:

$$M_k(i) = \sum_{j=1}^{i} j^k p_j \ , \tag{11}$$

where i is a frequency index and p_j is the discrete analog of Eq. (6).

Adaptive Learning Network

The basic structure of an adaptive learning network (ALN) is a cascade of building blocks. Each building block has two inputs, x_i and x_j, and one output, x_k, where:

$$x_k = a_o + a_1 x_i + a_2 x_j + a_3 x_i^2 + a_4 x_i x_j + a_5 x_j^2 \ . \tag{12}$$

The coefficients and specific network construction are determined by a training algorithm similar to that described by Mucciardi[1].

Before the training process begins, the data are grouped into three sets: a training set, a testing set, and a verification set. The training set is used to calculate the coefficients of each building block, the testing set is used to determine if a particular building block should be retained, and the verification set is used to test the final network on new data. Each data point consists of n vectors, or numbers, from test data which characterize that point. During the training process, all possible vector pairs from the training set are combined as shown in Eq. (12). Associated with each data point in the testing set is the desired output at that point, y. For each vector pair, the coefficients of the building block are determined to minimize mean squared error between calculated output of the ALN building block, x_k, and desired output, y. The corresponding vectors in the testing set are used as input to this building block. If the calculated outputs from both the training set and testing set are close enough to the corresponding desired output, the new building block is kept, along with its output, the new vector x_k.

In this manner, a new group of vectors is generated from the best combinations of the original vectors. The new vectors can be put through the same process. This process can be continued to as many levels as desired, usually until overfitting occurs. Typically, two to three levels of building blocks are generated for the final network.

For our particular problem, the original data consisted of a 20 μsec time-domain waveform for each of the 500 circumferential positions around the pipe. To generate vector inputs to the ALN, various operations were performed on these waveforms, such as peak voltage, fourier transforms, and second moment. We selected 20 input vectors that we thought were possibly significant. These 20 numbers, or vectors, characterized each circumferential position.

For a typical network training process, we selected 20 positions, or points, for the training set, 20 different points for the testing set, and the remaining 460 points for verification. In the training set, 2 points were selected from one 50% notch, 2 more from one 25% notch, and the remaining 16 from no-notch positions. The testing set was chosen similarly, using different points. Two notches were left for verification. The desired output is determined by:

$$Y = (2)(\text{notch depth}) \ . \tag{13}$$

Thus, the ideal output waveform would have a peak of height 1.0 for a 50% notch, a peak of height 0.5 for a 25% notch, and a zero elsewhere.

As mentioned previously, the coefficients for each building block are determined to minimize mean squared error between the desired output and calculated output using vector inputs from the training data. That is,

$$\text{Error} = \sum_{n=1}^{20} (x_{kn} - y_n)^2 \qquad 1/2 \tag{14}$$

$$x_{kn} = a_o + a_1 x_{in} + a_2 x_{jn} + a_3 x_{in}^2 + a_4 x_{in} x_{jn} + a_5 x_{jn}^2 \ , \tag{15}$$

where x_{in} is the i^{th} vector from the n^{th} point in the training set, and x_{jn} is the j^{th} vector from the n^{th} point in the training set.

Results

Isometric plots of detected waveform amplitude from Eq. (1), cross-correlation algorithm results from Eq. (4), and frequency domain power spectral density from Eq. (6) are compared in Figure 4 for the 60° refracted longitudinal scan. The peak voltage and cross-correlation results are presented here for about the same time domain window, and this window, 20 μsec wide, corresponds to a propagation path from the back surface through parent material, across the weld zone boundary, and through the weld zone to the top surface of the specimen (as illustrated in Fig. 2). The weld zone interface is visible as a ridge on the time domain records. Note that the ID surface echo is visible from circumferential position 190 through 310. The pipe was not perfectly round, and this caused the skew as the water path distance increased from 190 to 310.

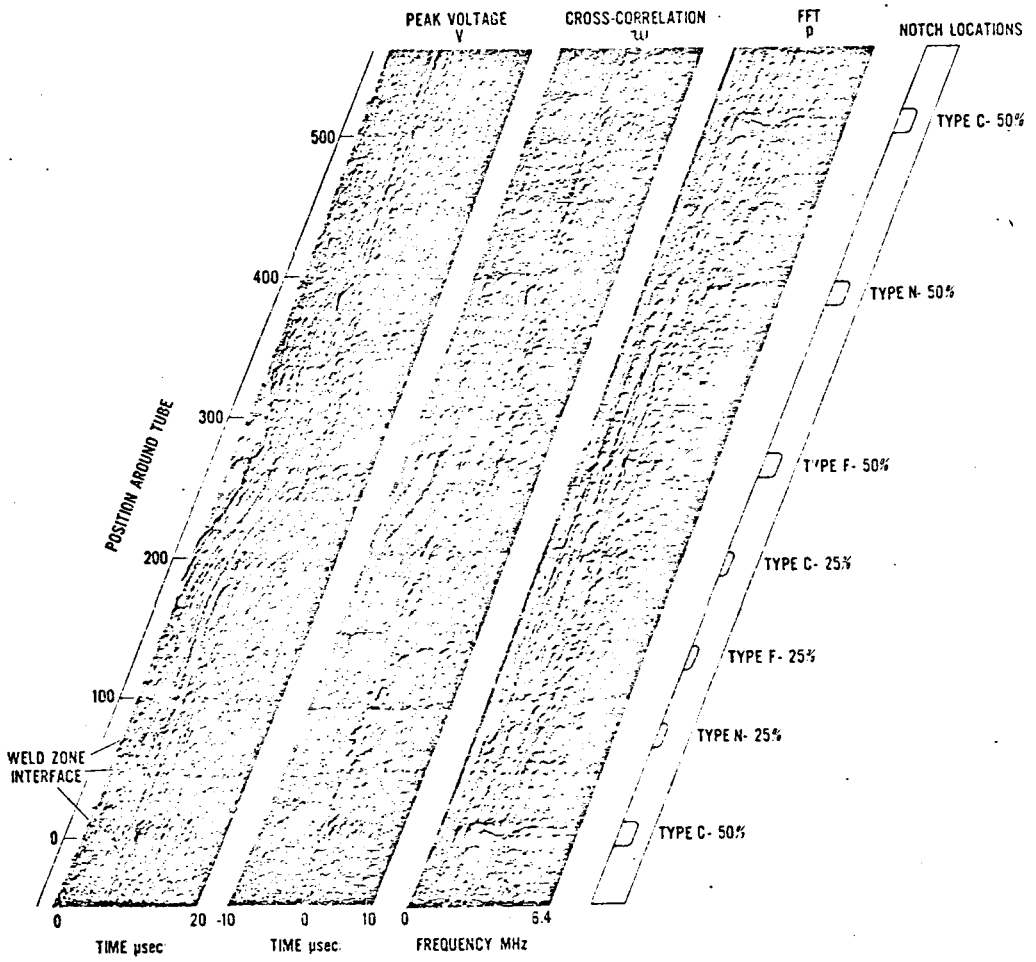

Fig. 4. Isometric Plots of Weld Zone UT Data for 60° Refracted Longitudinal Inspection.

The time domain plot from the cross-correlation algorithm contains less clutter than the peak voltage plot. Particularly, note the enhanced detail of the notches as compared to the ID surface echo and weld zone interface echo. Also, we find the notch type (near side, center, or far side) can be confirmed by noting the location in time of signal peaks with respect to the ridge from the weld zone interface.

The frequency domain data presented in Fig. 4 show a broadband response is received at each of the notch locations. We find this broadband response is typical of clean or distinct echos. Note the interference structure that is visible as frequency domain peaks in the vicinity of the larger notches. Although this structure was not analyzed in this study, we expect it should be predictable from the notch angle and type, as has been demonstrated by other investigators[14,15].

The attenuation influence of the weld zone is also visible from the frequency domain data plot. Specifically, near side notches show more information than do far side notches. This is expected because attenuation of the weld zone is progressively more severe at higher frequencies, and the wave path to far side notches traverses the most weld zone material.

Since a voltage peak can occur and will be reported in the time domain regardless of the frequency of the signal, and many of these peaks are from narrow band signals, the second order moment is more sensitive to broadband signals, indicative of the reflectors being sought. Therefore, the moment results illustrated in Fig. 5 are useful to show how energy is distributed.

Radiographic analysis from this pipe were compared to second order moment results and most all "non-notch" peaks were found to be associated with slight porosity within the weld zone.

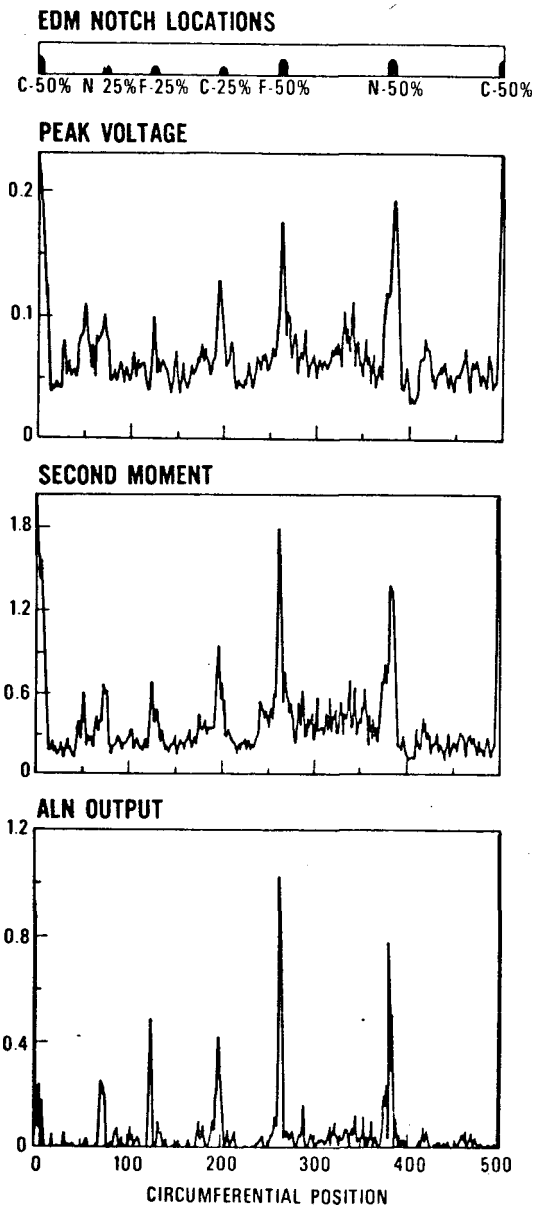

Fig. 5. Comparison of Peak Voltage Second Moment and ALN.

An ALN was generated using the data from the 60° refracted longitudinal scan. The notches at locations 262 and 125 were in the training set, those at 1 and 196 were in the testing set, and those at 72 and 383 were in the verification set. The resulting output is the average of three third-level vectors depicted in Fig. 5. The notches in the verification set were located successfully. All peaks not associated with the notches were lower in amplitude than the notch peaks.

A comparison of the ALN output to peak voltage and second moment results indicates significant improvement. Grain noise has been virtually eliminated and peaks from porosity are considerably smaller than with peak voltage or second moment.

Conclusion

Classical test methods, which compare signal amplitude to that from known reflectors, are not recommended for austenitic stainless steel welds. Peak voltages from "grain scatter" were often as large as signals from defects, and this would result in erroneous defect reports. Signals from notches were often buried in grain noise and these defects would be missed by classical test methods. It should be realized that our comparison here is for broadband testing. We would expect some improvement in classical signal amplitude correlation with defects if the test were narrow band and in the proper frequency range. Broadband results, specifically the isometric plots of frequency response, would be a proper tool to deduce the appropriate narrow band range to choose.

Analytical techniques have been developed and demonstrated that improve on conventional UT pre-service and in-service processes. Utilization of frequency domain information, specifically the M_2 algorithm, produces a better signal process defect indicator than time domain information. Combinations of both time and frequency domain information in an adaptive learning network produced results superior to any single process.

Acknowledgements

The authors would like to thank R. G. Chafin, C. J. Fewell, O. K. Selle and M. M. Sugiyama for their technical assistance in conducting this program, and A. L. Smith for interpreting the radiographic films of the tube section used in this study. We would also like to acknowledge the valuable technical discussions with Dr. W. P. Mech, Chairman, Mathematics Department at Boise State University, Boise, Idaho, and the continuing support and constructive review of this program by D. F. Young. Additionally, the assistance of N. E. Dixon in supplying transducer expertise is appreciated.

References

1. Mucciardi, A.N., Chang, J.K. and Lawrie, W.E., "Development of Adaptive Learning Networks for Pipe Inspection: Task I, Defect Versus Geometrical Reflector Discrimination in 304 Stainless Steel," Adaptronics, Inc., 1976.
2. Caussin, P., "Ultrasonic Testing of Austenitic Stainless Steel Structures," Association Vincotte, B-1640, Rhode-Saint-Genese, Belgigue, September 1976.
3. Peterson, R.O., Spanner, J.C. and Mech, S.J., "Development of Ultrasonic Method for Examining Stainless Steel Welds: Interim Progress Report," HEDL-TME 75-134, Hanford Engineering Development Laboratory, Richland, WA, November 1975.
4. McElroy, J.T., "Detailed Analysis of Fundamental Ultrasonic Response Data from Stainless Steel Corrosion Crack Specimens: Final Report," EPRI Tech. Planning Study 15-26 and SWRI Int. Res. Proj. 17-9183, San Antonio, TX, June 1976.
5. Holmes, E. and Beasley, D., "The Influence of Microstructure in the Ultrasonic Examination of Stainless Steel Welds," J. of Iron and Steel Inst., Vol. 200, pp. 283-290, April 1962.
6. Tomlinson, J.R., Wagg, A.R. and Whittle, M.J., "Ultrasonic Inspection of Austenitic Welds," presented at 2nd International Conference on Nondestructive Evaluation in the Nuclear Industry, Salt Lake City, UT, February 1978.
7. Kupperman, D.S., Reimann, K.J. and Fiore, N.F., "Role of Microstructure in Ultrasonic Inspectability of Austenitic Stainless Steel Welds," Materials Evaluation, 36, 5, 1978.
8. Herberg, G., Muller, W. and Ganglbauer, O., "Preliminary Results for Practical Ultrasonic Testing of Austenitic Steel Welds," NDT International, pp. 239-241, October 1976.
9. Wustenburg, H. and Mundry, E., "Limiting Influences on the Reliability of Ultrasonic Inservice Inspection Methods," Periodic Inspection of Pressurized Components, CP8, Ins. of Mech. Engrs., London, England, June 1974.
10. Beauchamp, K.G., Signal Processing Using Analog and Digital Techniques, Halstead Press, p. 412, 1973.
11. Bath, M., "Spectral Analysis in Geophysics," Developments in Solid Earth Geophysics, 7 Elsevier, p. 71, 1974.
12. Cooley, J.W., Lewis, P.A. and Welch, P.D., "Historical Notes on the Fast Fourier Transform," IEEE Transactions on Audio and Electroacoustics, Vol. AU-15, No. 2, 1967.
13. Bracewell, R.M., The Fourier Transform and Its Applications, McGraw-Hill, p. 138, 1965.

14. Gilmore, R.S. and Czerw, G.J., "The Use of Radiation Field Theory to Determine the Size and Shape of Unknown Reflectors by Ultrasonic Spectroscopy," Materials Evaluation, Vol. 35, No. 1, pp. 37-45, January 1977.

15. Adler, L., Cook, K.V., Shaley, H.L. and McClung, R.W., "Flaw-Size Measurement in a Weld Sample by Ultrasonic Frequency Analysis," Materials Evaluation, Vol. 35, No. 3, pp. 44-50, March 1977.